# Carbon nanotube woven textile photodetector

Ahmed Zubair,[1] Xuan Wang,[1] Francesca Mirri,[2] Dmitri E. Tsentalovich,[2] Naoki Fujimura,[3] Daichi Suzuki,[3] Karuppasamy P. Soundarapandian,[4] Yukio Kawano,[3] Matteo Pasquali,[2,5,6,*] and Junichiro Kono[1,5,7,†]

[1]*Department of Electrical and Computer Engineering, Rice University, Houston, Texas 77005, USA*
[2]*Department of Chemical and Biomolecular Engineering, Rice University, Houston, Texas 77005, USA*
[3]*Quantum Nano-electronics Research Center, Department of Electrical and Electronic Engineering, Tokyo Institute of Technology, Meguro-ku, Tokyo 152-8552, Japan*
[4]*Department of Physics and Nanotechnology, SRM University, Chennai, Tamil Nadu 603203, India*
[5]*Department of Materials Science and NanoEngineering, Rice University, Houston, Texas 77005, USA*
[6]*Department of Chemistry, Rice University, Houston, Texas 77005, USA*
[7]*Department of Physics and Astronomy, Rice University, Houston, Texas 77005, USA*

(Received 26 September 2017; published 24 January 2018)

The increasing interest in mobile and wearable technology demands the enhancement of functionality of clothing through incorporation of sophisticated architectures of multifunctional materials. Flexible electronic and photonic devices based on organic materials have made impressive progress over the past decade, but higher performance, simpler fabrication, and most importantly, compatibility with woven technology are desired. Here we report on the development of a weaved, substrateless, and polarization-sensitive photodetector based on doping-engineered fibers of highly aligned carbon nanotubes. This room-temperature-operating, self-powered detector responds to radiation in an ultrabroad spectral range, from the ultraviolet to the terahertz, through the photothermoelectric effect, with a low noise-equivalent power (a few $\mathrm{nW/Hz^{1/2}}$) throughout the range and with a $ZT$-factor value that is twice as large as that of previously reported carbon nanotube-based photothermoelectric photodetectors. Particularly, we fabricated a $\sim$ 1-m-long device consisting of tens of $p^+$-$p^-$ junctions and weaved it into a shirt. This device demonstrated a collective photoresponse of the series-connected junctions under global illumination. The performance of the device did not show any sign of deterioration through 200 bending tests with a bending radius smaller than 100 $\mu$m as well as standard washing and ironing cycles. This unconventional photodetector will find applications in wearable technology that require detection of electromagnetic radiation.

DOI: 10.1103/PhysRevMaterials.2.015201

## I. INTRODUCTION

The field of wearable electronics and photonics [1–4] is advancing rapidly in response to the increasing societal needs for monitoring, sensing, and processing information in a dynamic, personal, and pervasive manner. Thus, smart textiles based on seamless device integration into clothing is anticipated to dominate the wearable technology field in the near future. Fiber-based designs are well suited for wearable devices as they can be easily woven into textiles and preserve the inherent comfort of fabrics. Owing to this advantage, different fiber-based wearable electronic devices like transistors [5], antennas [6], pressure sensors [7], biosensors [8], energy harvesters [9], and energy storage devices [10] have been reported. In particular, wearable photodetectors have a great potential for personal, military, and space wear applications, allowing electromagnetic wave detection and energy harvesting. Photodetector devices that can be bent, folded, and stretched have been fabricated in a two-dimensional configuration by using thin films of various types of materials [11–18]. However, these film photodetectors are not compatible with conventional textile technology due to the need of substrate support rather than direct integration into clothing.

Furthermore, smart textiles for electronic and medical applications face the challenges of providing power to the wearable devices. A previously reported photovoltaic fiber, consisting of a dye-sensitized solar cell structure deposited on an optical fiber, needed light to be coupled into the end of the fiber and could not be readily incorporated into textiles [19]. Monolithic-structured textile-based solar cells with a complex fabrication process have been demonstrated [20]. Silicon $p$-$i$-$n$ junction based fibers have limited potential because of difficulties in fabricating layers inside the capillary pore of a silica fiber [21]. An organic solar cell based on poly(3-hexylthiophene) (P3HT) : 1-(3-methoxycarbonyl)-propyl-1-phenyl-(6,6)$C_{61}$ (PCBM) has been fabricated onto an optical fiber [10]. However, self-standing and easily incorporable textile solar cells and photodetectors have not been reported.

Recently, carbon nanotube (CNT) fibers, characterized by high electrical and thermal conductivity, light weight, high mechanical strength, flexibility, bending fatigue resistance, and superb environmental stability, have been produced [22,23]. Vast utilization of these properties in macroscopic devices is predicted for the near future [24]. There have been several studies on the use of the photothermoelectric (PTE) effect in CNTs for photodetection based on aligned and unaligned networks of single wall and double wall CNTs [25–27]. Moreover, CNTs

*mp@rice.edu
†kono@rice.edu

 

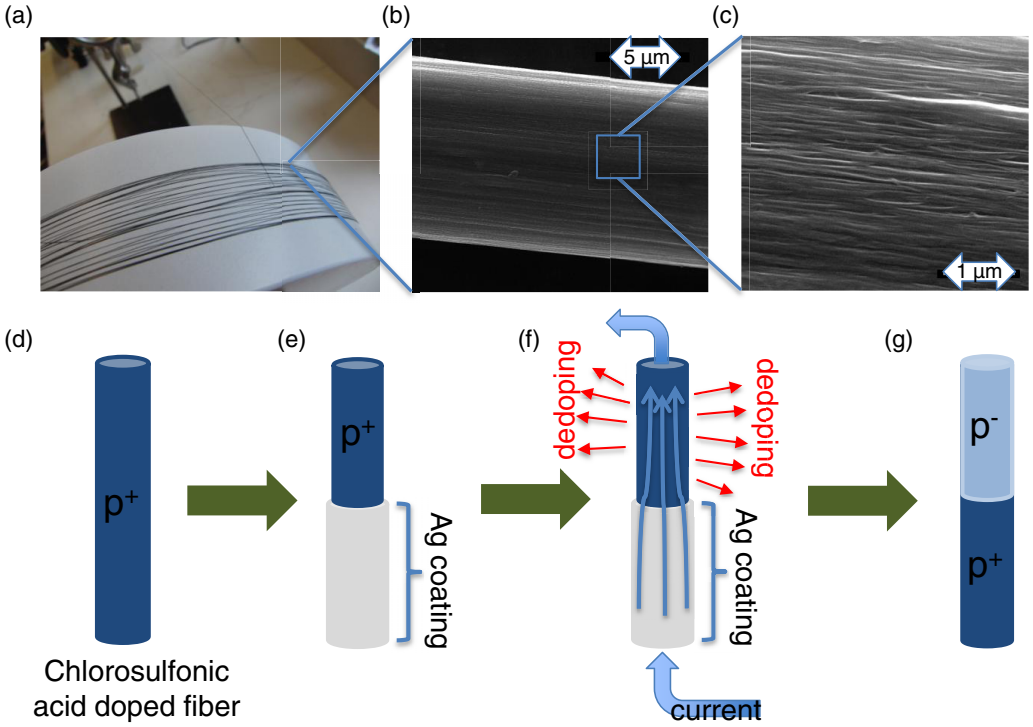


FIG. 1. Doping-engineered fibers of aligned CNTs. (a) Ultralong CNT fiber on a winding drum. (b) Magnified optical image of the fiber. (c) Scanning electron microscopy (SEM) image showing well-aligned CNTs inside the fiber. (d) As prepared CNT fiber, which is heavily $p$ doped. (e) A piece of CNT fiber partially coated by silver paint. (f) Selective current annealing. A large current passes through the silver coating layer on the bottom portion but directly through the CNT fiber in the upper portion, inducing dedoping (i.e., removal of dopants). (g) After removing the silver paint, the fiber has a $p^+$-$p^-$ junction.

absorb broadband polarized light from the ultraviolet to the far-infrared wavelengths [27,28], making CNT fibers an ideal material for wearable optoelectronic devices.

Here we developed PTE effect-based, flexible, substrate-free, polarization-sensitive, room-temperature, and biasless photodetectors that work from the ultraviolet to the terahertz. Therefore, whenever there is absorption of electromagnetic radiation, which creates a temperature gradient, a thermoelectric voltage will be produced. We integrated this CNT-fiber photodetector into textiles by simply sewing it into fabric, creating "smart" shirts that can harvest sunlight as well as detect light on a moving human body. The smart shirt showed mechanical robustness under severe deformation conditions and can be washed, dried, and ironed without any change in performance. These low-cost, ultrabroadband, and wearable photodetectors are promising for a wide range of applications in flexible optoelectronics, astronomy, sensing, spectroscopy, imaging, defense, and communications.

## II. METHODS

### A. CNT fiber manufacturing

The wet spinning method was used to manufacture the CNT fibers [22,29]. High-quality CNTs purchased from Cabon Nanotechnologies, Inc., Unidym, Inc., Teijin Aramid BV, and Meijo Nano Carbon Co., Ltd were dissolved in chlorosulfonic acid at a concentration of 2 to 6 wt.% forming liquid crystals [30,31]. The liquid crystal solution was extruded through a spinneret (65 to 130 $\mu$m in diameter) into a coagulant to remove the acid. The forming filament was collected onto a winding drum. The linear velocity of the drum was higher than the extrusion speed at the spinneret exit, to ensure high CNT alignment by continuous stretching and tensioning of the filament. Then the fibers were stabilized in the oven for 24 h at 115 °C and washed in warm water (50 °C) for 3 h. These fibers were heavily $p$ doped ($p^+$ doped) due to the uncomplete solvent removal. The 3-ply CNT rope was manufactured by simultaneously spinning seven filament fiber bundles and then plying three such bundles together.

### B. Photodetector fabrication

Inherently $p$-doped fibers can be made less $p$ doped by partially removing the dopants through annealing. As shown in Fig. 1(e), we covered only one side of the fiber with silver paint, which has a higher conductance than the CNT fiber. We then flowed a high current for current annealing [Fig. 1(f)]. On the side coated by silver, most of the current only passes through the silver paint, and thus nothing happens in the CNT fiber. On the uncoated side, the large current goes directly through the CNT fiber, which results in annealing and dedoping. After this step, we used acetone to dissolve the silver paint and brushed off the silver paint using a cotton-tip, which left a $p^+$-$p^-$ junction in the middle [Fig. 1(g)]. We used a Keithley 2400 sourcemeter as a current source, and a temperature controller to control and monitor the temperature of the sample chamber. The current annealing procedure was done in a nitrogen environment. The chamber was evacuated

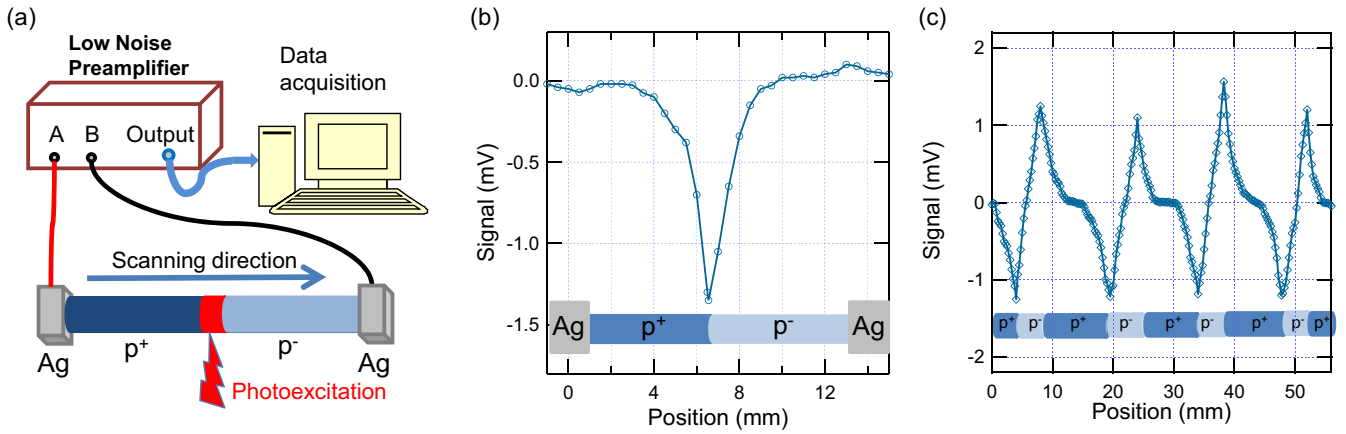


FIG. 2. Position-dependent photoresponse of the CNT-fiber photodetectors. (a) Experimental setup for scanning photovoltage measurements. Experimental results are shown for (b) CNT-fiber $p^+$-$p^-$ photodetector and (c) multiple $p^+$-$p^-$ junction CNT fiber photodetector. Schematic of each device is shown inside each panel.

(∼2 mTorr), and then compressed nitrogen gas was introduced into the chamber. This is a novel approach for creating a junction in the fiber. In the same way, multiple junctions were formed in a single fiber by alternatively covering one portion of the fiber and then current annealing. The photodetector was suspended in air, and G10 plastic was used as the suspending material for the two ends of the fiber. Two electrodes were made by using silver paste on the two edges of the device.

### C. Device characterization

Ultraviolet, visible, and near-infrared radiation was produced using laser diodes at 405, 660, and 1350 nm, respectively. Mid-infrared radiation was produced using a tunable quantum cascade laser at 4.3 to 4.7 $\mu$m. A far-infrared molecular gas laser with several lines was used for producing terahertz radiation. To obtain the attenuation spectrum of the CNTs, we used UV-VIS-NIR absorption spectroscopy and Fourier transform infrared (FTIR) spectroscopy. From UV-VIS-NIR absorption spectroscopy, we measured attenuation from 300 nm to 2 $\mu$m wavelength range. We used two detectors (TGS and PETGS) for measurements from 1.4 to 92 $\mu$m wavelength range in the FTIR spectroscopy system. For noise voltage measurements, the electrical voltage of the device was amplified by a low-noise voltage amplifier and then fed into a lock-in amplifier. A noise signal with a certain central frequency and bandwidth was extracted from the total voltage signal. The noise voltage was transformed into a dc voltage with a low-pass filter, which was multiplied by an amplifier.

## III. RESULTS AND DISCUSSION

CNT fibers of 10–25 $\mu$m diameter [Fig. 1(a)] were manufactured using a wet spinning method that consists of dissolving CNTs in chlorosulfonic acid and extruding the solution through a spinneret in a coagulation bath [22]. Scanning electron microscopy (SEM) images [Figs. 1(b) and 1(c)] of the fiber show strong alignment inside the fiber due to the shear applied during spinning and the liquid crystalline nature of the CNT solution. CNT fibers are heavily $p$-type doped (referred to as "$p^+$ doped" in the following) by chlorosulfonic acid used during the production process, which can be removed by annealing the fibers at high temperature (see Sec. II). In order to maximize the PTE [25–27,32] (whose mechanism is described in detail in the Supplemental Material [33]), we created $p^+$-$p^-$ junctions, where the Seebeck coefficient $S$, defined as the thermoelectric voltage produced per unit temperature difference across the material junction, suddenly changes and so its spatial gradient $dS/dx$ is maximized. As shown in Figs. 1(d)–1(g) (and described in Sec. II), we used current annealing to make these junctions.

A scanning photovoltage microscopy setup, schematically shown in Fig. 2(a), was used to measure the spatial dependence of the photovoltage of the doping-engineered CNT fibers. We used a 660 nm laser diode, and all measurements were performed in air and at room temperature. Figure 2(b) shows the photovoltage of the $p^+$-$p^-$ CNT fiber detector as a function of the position of the focused laser beam along the detector. The voltage magnitude is maximum at the junction and monotonically decreases in both directions due to exponentially decaying temperature profile by local heating of the laser beam. Figure 2(c) shows the spatially dependent voltage response of a multiple-junction device. The measured voltage shows opposite signs at $p^+$-$p^-$ and $p^-$-$p^+$ junctions, as expected due to the opposite gradient of the Seebeck coefficient when they are locally illuminated with the laser beam.

To leverage the unique fact that our flexible CNT-fiber detector does not require any substrate and operates without any external power, we fabricated a textile photodetector by directly sewing it into a shirt [Figs. 3(a)–3(c)]. We produced a ∼1-m-long CNT rope of an average diameter of 135 $\mu$m by braiding 21 CNT fibers. We created 64 junctions (32 $p^+$-$p^-$ and 32 $p^-$-$p^+$ junctions) by using the selective current annealing method described in Figs. 1(d)–1(g). As seen in Fig. 2(c), adjacent junctions have opposite photovoltage signs, and thus the device was sewn in such a way that every other junction was hidden under the cloth [Fig. 3(d)]. Global illumination of the device with broadband white light [Fig. 3(e)] induces a photovoltage response, as illustrated by the $I$-$V$ characteristics of the device with and without illumination in Fig. 3(f). This is because all the junctions exposed have the same sign of photovoltage, and thus their contributions do not cancel each

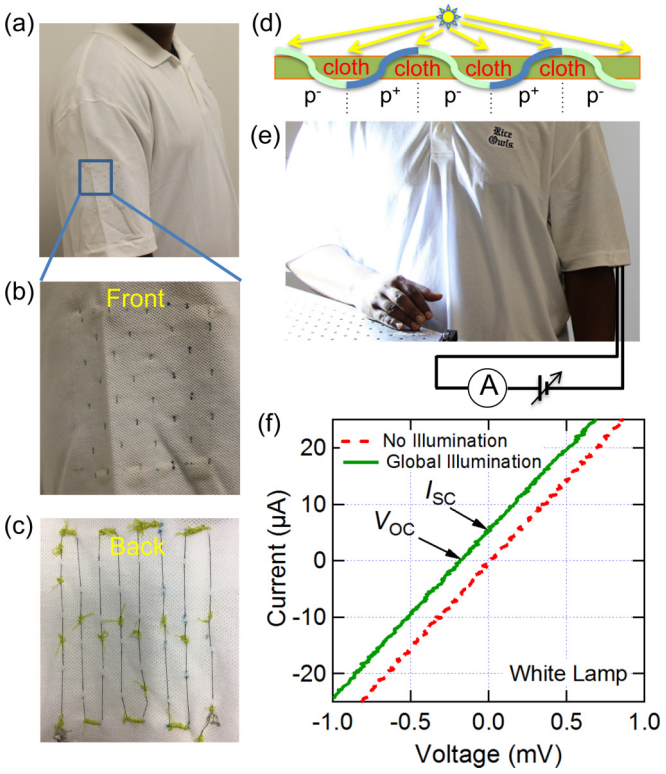


FIG. 3. CNT-weaved shirt photodetector. (a) Flexible, wearable CNT fiber detector sewed into a polo shirt. (b) The front side of the detector, i.e., the active portion that is illuminated. (c) The back side of the detector, which is inside of the shirt. (d) The fiber is sewn in such a way that the $p^+$-$p^-$ junctions are outside the shirt and exposed to light while the $p^-$-$p^+$ junctions are hidden inside the shirt. (e) The ends of the fiber detector are connected to an external circuit for measuring the induced photovoltage. (f) The $I$-$V$ characteristics of the detector under no illumination and global illumination by a white lamp. The $I$-$V$ curve shifts upward as it harvests power under illumination.

other. Note that the photovoltage in Fig. 3(f) is not a result of cloth absorption, but rather because of the temperature difference between the covered and uncovered portions of the CNT fiber. Having more series junctions greatly enhances the signal compared to a single junction due to the addition of the photovoltages generated at the individual junctions. The $I$-$V$ curve rigidly shifts upward, harnessing power, i.e., producing an open-circuit photovoltage ($V_{OC}$) and a short-circuit photocurrent ($I_{SC}$), acting as a wearable solar cell. This is a distinguishing characteristic of a PTE-based photodetector, distinct from photodiodes, photoconductors, and bolometers.

We used a variety of optical sources to investigate the wavelength dependence of the photoresponse. Figure 4(a) shows the typical photoresponse of our CNT-fiber detector to 405-nm-wavelength ultraviolet radiation. Under illumination, the $I$-$V$ curve shifts, creating finite $V_{OC}$ and $I_{SC}$, similar to what we observed under white-light illumination [Fig. 3(f)]. Essentially the same behavior is seen in $I$-$V$ characteristics when we illuminate the device with near-infrared [Fig. 4(b)], mid-infrared [Fig. 4(c)], and far-infrared [Fig. 4(d)] radiation. Data showing similar behavior at three other wavelengths are shown in Fig. S1 of the Supplemental Material [33]. This universal $I$-$V$ characteristic under illumination, from the ultraviolet to the terahertz, highlights the unique ultrabroadband response of this detector to electromagnetic radiation making this CNT sewable photodetector suitable for various diverse radiation environments.

To determine the responsivity of our CNT-fiber detector, we measured the photovoltage ($V_{OC}$) as a function of incident light power (shown in Fig. S1(d) of the Supplemental Material [33]). Figure S1(d) shows the open-circuit photovoltage of the detector as a function of incident power at 405 nm, 660 nm, 1350 nm, 4.53 $\mu$m, and 96.5 $\mu$m. For all the wavelengths, the response changes linearly with the power of the excitation beam.

From the slope of the power dependence characteristics, we can calculate the responsivity $\Re$, in V/W. We measured the $\Re$ at ultraviolet (405 nm), visible (660 nm), and near-infrared (1350 nm) wavelengths for a CNT-fiber detector that consisted of a single fiber. For the cases of mid-infrared (4.53 $\mu$m) and far-infrared (96.5 $\mu$m) excitation, we used a multiple-fiber detector. The multiple-fiber detector was fabricated by making 12 parallel fibers having $p^+$-$p^-$ junctions in each of them at the same spatial position and then by stacking eight such parallel fiber layers. From the attenuation spectrum [shown in Fig. 4(e) of the paper], we calculated the attenuation length for CNTs to be ~4.5 and ~0.9 $\mu$m at 4.53 and 96.5 $\mu$m wavelengths, respectively. As the attenuation lengths were less than the diameter of the fibers, all the incident power of the excitation beams was attenuated in the first layer of parallel fibers. To take into account the fact that these 12 fibers split the total incident power, we multiplied the measured photovoltage of the detector by 12 and calculated the $\Re$. The incident power was measured by subtracting the measured power with the detectors (powermeter located after the detectors) from the measured power without the detectors for all measurements. The $\Re$ values of CNT-fiber detectors at different wavelengths are reported in Table I. The obtained responsivities varied from ~160 to ~330 mV/W among different wavelengths.

A figure of merit for photodetectors is the noise equivalent power (NEP), which is the minimum detectable optical power corresponding to a signal-to-noise ratio of 1. We measured noise spectra for CNT-fiber photodetector devices to determine the NEP. The NEP is defined as

$$\text{NEP} = N/\Re, \tag{1}$$

where $N$ is the noise spectral density in units of $\text{V/Hz}^{1/2}$.

Our noise spectra measurements indicated that the zero-bias dark noise $N$ of CNT-fiber photodetectors reaches the Johnson noise limit. The NEP values of the CNT-fiber photodetector were calculated at 405 nm, 660 nm, 1350 nm, 4.53 $\mu$m, and 96.5 $\mu$m and shown in Table II. In the visible wavelength regime, the NEP of the fiber photodetector was found to be 4.4 $\text{nW/Hz}^{1/2}$. The NEP is 0.9 $\text{nW/Hz}^{1/2}$ in the THz range (3.11 THz or 96.5 $\mu$m), which is more than one order better than that of the PTE-based detector previously reported [26]. The NEP is in the range of a few $\text{nW/Hz}^{1/2}$ on average for our CNT-fiber detectors over an ultrabroad wavelength range—from the ultraviolet to the far-infrared. Furthermore, we can estimate another photodetector performance parameter,

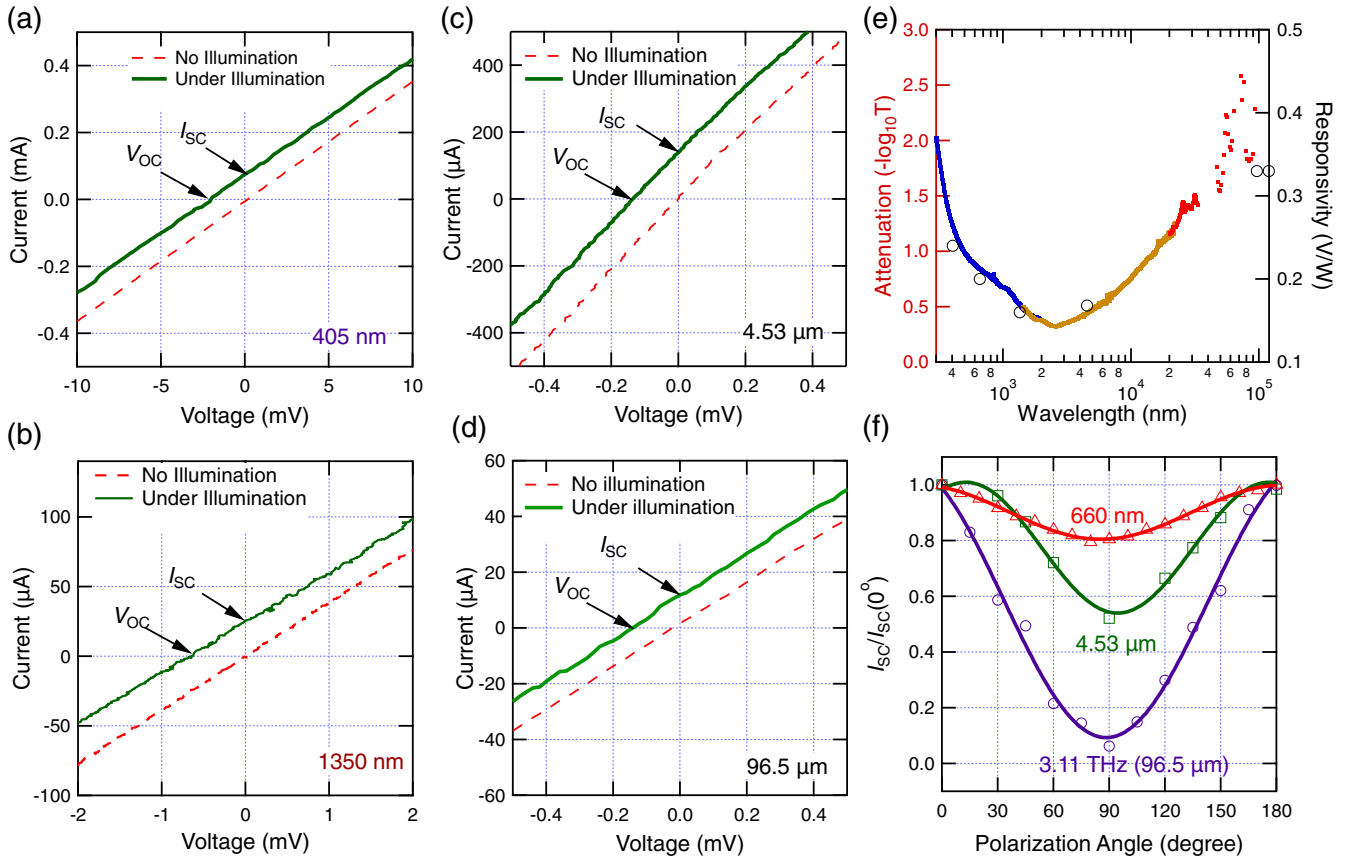


FIG. 4. Basic characteristics of the CNT-fiber detector. The $I$-$V$ characteristics of the photodetector with and without illumination in the (a) ultraviolet range (405 nm), (b) near-infrared range (1350 nm), (c) mid-infrared range (4.53 $\mu$m), and (d) far-infrared range (96.5 $\mu$m or 3.11 THz). The $I$-$V$ curve is always linear, and it rigidly shifts whenever the device is illuminated, resulting in a finite open-circuit voltage $V_{OC}$ and short-circuit current $I_{SC}$. (e) Attenuation (left axis) and responsivity (right axis) as a function of wavelength. Attenuation spectra is obtained using UV-VIS-NIR absorption spectroscopy (blue dots) and FTIR spectroscopy (brown dots using TGS detector and red dots using PETGS detector). (f) Polarization dependence of the short-circuit photocurrent at visible (660 nm), mid-infrared (4.53 $\mu$m), and far-infrared (96.5 $\mu$m) wavelengths.

specific detectivity $D^*$, using the following equation:

$$D^* = \frac{\sqrt{A_{\text{active}}}}{\text{NEP}}, \tag{2}$$

where $A_{\text{active}}$ is the active area of the device. The $D^*$ values for our photodetector are presented in Table II.

TABLE I. Responsivity $\Re$ of CNT-fiber detectors at different wavelengths.

| Regime | Wavelength ($\mu$m) | $\Re$ (V/W) |
|---|---|---|
| Ultraviolet | 0.405 | 0.24 |
| Visible | 0.66 | 0.2 |
| Near-infrared | 1.35 | 0.16 |
| Mid-infrared | 4.53 | 0.168 |
| Far-infrared | 96.5 | 0.33 |
| Far-infrared | 119 | 0.32 |
| Far-infrared | 215.8 | 0.32 |

A dimensionless figure of merit $ZT$, used to characterize the potential of thermoelectric materials, is given by

$$ZT = \frac{S_{\text{CNT}}^2 \sigma T}{\kappa_{\text{CNT}}}, \tag{3}$$

where $S_{\text{CNT}}$ is the Seebeck coefficient of CNTs, $\sigma$ is the conductivity of CNTs, $T$ is the temperature, and $\kappa_{\text{CNT}}$ is the thermal conductivity of the CNTs.

Our photodetector device have $ZT \approx 3.6 \times 10^{-4}$, which is twice the value of the previously reported CNT PTE photodetectors [34]. However, this $ZT$ value is quite small compared

TABLE II. NEP and $D^*$ of the CNT-fiber detectors at different wavelengths.

| Wavelength ($\mu$m) | NEP (nW/Hz$^{1/2}$) | $D^*$ (cmHz$^{1/2}$/W) |
|---|---|---|
| 0.405 | 3.7 | $3.03 \times 10^5$ |
| 0.660 | 4.4 | $2.52 \times 10^5$ |
| 1.350 | 5.5 | $2.02 \times 10^5$ |
| 4.530 | 1.8 | $2.20 \times 10^6$ |
| 96.50 | 0.9 | $4.33 \times 10^6$ |

to the value $ZT \approx 1$ for best thermoelectric materials. By increasing the electrical conductivity $\sigma$, we can reduce the noise voltage. Nevertheless, the photovoltage has an inversely proportional relation with $\sigma$. Therefore, the optimal $\sigma$ value could be determined in the future for the best performance. Again, we can deduce the relations $\Delta V \propto 1/G^{1/2}$, $\Delta V \propto 1/\kappa_{\mathrm{CNT}}^{1/2}$, and $\Delta V \propto 1/d^{3/2}$ [33]. Our experimental data illustrate that the photovoltage decreases with increasing diameter of our CNT-fiber photodetector (details of diameter dependence is also discussed in the Supplemental Material [33]). The performance of our CNT-fiber PTE photodetectors can be significantly improved by engineering the above mentioned parameters. We also described the properties of the CNTs used to fabricate our detectors and the temperature dependence of electrical conductivity for a $p^+$ fiber and a $p^-$ fiber in the Supplemental Material [33]. Previously we reported the temperature dependence of resistivity for doped ($p^+$) and de-doped ($p^-$) fibers manufactured using CNTs purchased from Teijin Aramid BV [35]. Also, we reported the electrical conductivities of doped and de-doped fibers produced using CNTs from Carbon Nanotechnologies, Inc. [22].

We also determined the performance of the device as a solar harvester [33]. As the $I$-$V$ curve shifts rigidly under illumination, the fill factor is 25%. The power conversion efficiency of our CNT-fiber photodetector is $4.4 \times 10^{-6}$, which is comparable to that of a previously reported photovoltaic fiber [19]. The external quantum efficiency was found to be ~0.8% [33].

To understand the wavelength dependence of the device photoresponse, we performed absorption measurements on a CNT film made from the same CNTs used for the CNT-fiber detector. Figure 4(e) shows the wavelength dependence of the attenuation of the film (blue, brown, and red dots, left axis), together with the responsivity of the CNT-fiber detector (black empty circles, right axis). The attenuation and responsivity spectra agree very well throughout the whole spectral range. The ultrabroadband absorption makes CNT-fiber detectors perfect for detection and energy harvesting from a very broad electromagnetic wavelength range. Furthermore, by making detectors from single-chirality CNTs, the detector could be made wavelength selective.

Another advantage of this detector is the polarization sensitivity, which is naturally built in because of the intrinsically anisotropic absorption properties of CNTs combined with the highly aligned nature of CNTs in these fibers [36]. As a demonstration, we measured the polarization dependence of the photoresponse at three wavelengths by changing the polarization angle of the incident electromagnetic wave, as shown in Fig. 4(f). In the terahertz range (96.5 $\mu$m), the polarization anisotropy is extremely large—the ratio of the $I_{\mathrm{SC}}$ value for perpendicular polarization to that for parallel polarization is ~6%. This is due to the fact that intraband, free-carrier response is intrinsically much more polarization dependent than interband absorption.

Finally, to explicitly demonstrate the flexibility and wearability of the CNT-fiber detector, we fabricated several devices with and without a flexible substrate-PTFE (Teflon), as shown in Figs. 5(a)–5(d), and we bent and straightened them multiple times. We performed bending tests on three devices, during which the devices were completely folded. The performance

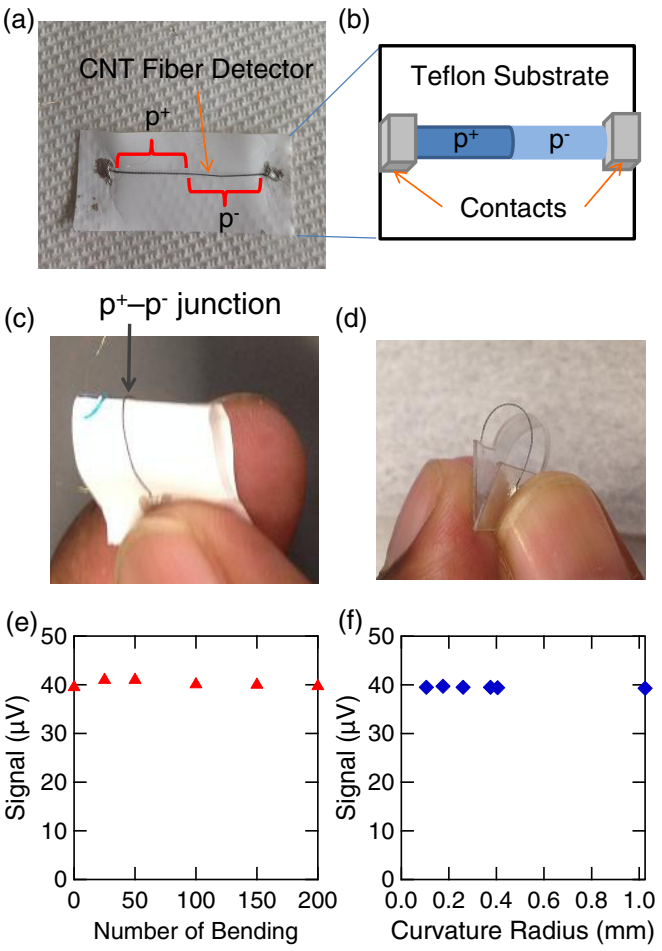


FIG. 5. Flexibility tests of the CNT-fiber detectors. (a) CNT-fiber detector on a Teflon substrate. (b) Schematic diagram of the sample device setup. Flexibility is shown for a device on Teflon (c) and suspended in air (d). (e) Photovoltage as a function of number of bending cycles, showing a constant voltage even after 200 cycles. The detector was completely bent during bending tests. (f) Photovoltage for different bending curvatures, showing that the signal does not deteriorate even with a bending curvature of 100 $\mu$m.

of all CNT-fiber devices did not change even after 200 bending tests [Fig. 5(e)]. The bend radius was less than 100 $\mu$m, but the measured photoresponse of the detectors did not change during the bending tests, as shown in Fig. 5. These bending tests demonstrate the superior mechanical resilience of the CNT-fiber detector compared to previously reported fiber-based solar cells [20,21]. The tensile strength of the CNT fibers was found to be ~0.8−2.5 GPa. Hence, our device works as a robust flexible optoelectronic component, being able to detect light or harvest power during severe deformations.

We also washed, dried, and ironed the textile photodetector shown in Fig. 3(a) [33]. The performance of the photodetector remains the same after a whole laundry cycle of washing, drying, and ironing. Their flexibility, light weight, and ease in incorporating them into textiles on human bodies make the CNT-fiber photodetectors extremely promising in the wearable electronics field.

## IV. CONCLUSIONS

We developed a sewable, substrateless, polarization-sensitive photodetector using CNT fibers. This ultrabroadband photodetector has a low noise-equivalent power and shows no sign of performance degradation after flexibility tests. We demonstrated the wearability of this device by creating a smart shirt that can be washed, dried, and ironed with no change in performance. The promising properties of this device open the route for seamlessly integrated photodetectors for the rapidly growing wearable technology field.

## ACKNOWLEDGMENTS

We thank Colin C. Young, Xiaowei He, Weilu Gao, and Robert J. Headrick for technical assistance and useful discussions. A.Z. and J.K. were supported by DOE BES DE-FG02-06ER46308 (THz characterization of CNT fibers), NSF ECCS-1708315 (device fabrication), the Robert A. Welch Foundation Grant No. C-1509 (sample preparation), and the W. M. Keck Foundation. D.E.T., F.M., and M.P. were supported by AFOSR through Grant No. FA9550-15-1-0370 and the Robert A. Welch Foundation Grant No. C-1668. N.F., D.S., and Y.K. were supported by Collaborative Research Based on Industrial Demand, the JST-Mirai Program, the Matching Planner Program, and the Center of Innovation Program from the Japan Science and Technology Agency, JSPS KAKENHI Grants No. JP16J09937, No. JP17K19026, No. JP17H02730, No. JP16H00798, and No. JP16H00906 from Japan Society for the Promotion of Science, the Murata Science Foundation, and Support for Tokyo tech Advanced Researchers (STAR). The authors declare the following competing financial interest(s): M.P., D.E.T., and F.M. are authors of the PCT international application PCT/EP2012/067478 describing the method for manufacturing fibers of carbon nanotubes by wet spinning. M.P., D.E.T., and F.M. have a financial interest in DexMat, Inc., which is commercializing wet-spun carbon nanotube fibers.

[1] X. Tao, Ed., *Wearable Electronics and Photonics* (CRC, Taylor & Francis, Boca Raton, FL, 2005).
[2] S. Poslad, *Ubiquitous Computing: Smart Devices, Environments and Interactions* (Wiley, New York, 2009).
[3] S. Greengard, *The Internet of Things* (The MIT Press, Cambridge, MA, 2015).
[4] F. Cicoira and C. Santato, Eds., *Organic Electronics: Emerging Concepts and Technologies* (Wiley, New York, 2013).
[5] D. De Rossi, Nat. Mater. **6**, 328 (2007).
[6] Z. Wang, L. Zhang, Y. Bayram, and J. L. Volakis, IEEE T. Antenn. Propag. **60**, 4141 (2012).
[7] W. Zeng, L. Shu, Q. Li, S. Chen, F. Wang, and X.-M. Tao, Adv. Mater. **26**, 5310 (2014).
[8] J. Yoo, L. Yan, S. Lee, Y. Kim, and H. J. Yoo, IEEE J. Solid-State Circ. **45**, 178 (2010).
[9] S. Pan, Z. Yang, H. Li, L. Qiu, H. Sun, and H. Peng, J. Am. Chem. Soc. **135**, 10622 (2013).
[10] J. Liu, M. A. G. Namboothiry, and D. L. Carroll, Appl. Phys. Lett. **90**, 063501 (2007).
[11] T. Sekitani and T. Someya, Adv. Mater. **22**, 2228 (2010).
[12] S.-I. Park, A.-P. Le, J. Wu, Y. Huang, X. Li, and J. A. Rogers, Adv. Mater. **22**, 3062 (2010).
[13] Y. Liu, H. Zhou, R. Cheng, W. Yu, Y. Huang, and X. Duan, Nano Lett. **14**, 1413 (2014).
[14] N. Liu, H. Tian, G. Schwartz, J. B. H. Tok, T.-L. Ren, and Z. Bao, Nano Lett. **14**, 3702 (2014).
[15] D. De Fazio, I. Goykhman, D. Yoon, M. Bruna, A. Eiden, S. Milana, U. Sassi, M. Barbone, D. Dumcenco, K. Marinov, A. Kis, and A. C. Ferrari, ACS Nano **10**, 8252 (2016).
[16] Z. Zheng, T. Zhang, J. Yao, Y. Zhang, J. Xu, and G. Yang, Nanotechnology **27**, 225501 (2016).
[17] X. Liu, E. K. Lee, D. Y. Kim, H. Yu, and J. H. Oh, ACS Appl. Mater. Interfaces **8**, 7291 (2016).
[18] T. Yokota, P. Zalar, M. Kaltenbrunner, H. Jinno, N. Matsuhisa, H. Kitanosako, Y. Tachibana, W. Yukita, M. Koizumi, and T. Someya, Sci. Adv. **2**, e1501856 (2016).
[19] M. Toivola, M. Ferenets, P. Lund, and A. Harlin, Thin Solid Films **517**, 2799 (2009).
[20] M. J. Yun, S. I. Cha, H. S. Kim, S. H. Seo, and D. Y. Lee, Sci. Rep. **6**, 34249 (2016).
[21] R. He, T. D. Day, M. Krishnamurthi, J. R. Sparks, P. J. A. Sazio, V. Gopalan, and J. V. Badding, Adv. Mater. **25**, 1461 (2013).
[22] N. Behabtu, C. C. Young, D. E. Tsentalovich, O. Kleinerman, X. Wang, A. W. K. Ma, E. A. Bengio, R. F. ter Waarbeek, J. J. de Jong, R. E. Hoogerwerf, S. B. Fairchild, J. B. Ferguson, B. Maruyama, J. Kono, Y. Talmon, Y. Cohen, M. J. Otto, and M. Pasquali, Science **339**, 182 (2013).
[23] A. Zubair, D. Tristant, C. Nie, D. E. Tsentalovich, R. J. Headrick, M. Pasquali, J. Kono, V. Meunier, E. Flahaut, M. Monthioux, I. C. Gerber, and P. Puech, Phys. Rev. Mater. **1**, 064002 (2017).
[24] H. Peng, Q. Li, and T. Chen, Eds., *Industrial Applications of Carbon Nanotubes* (Elsevier, Amsterdam, 2017).
[25] S. Nanot, A. W. Cummings, C. L. Pint, A. Ikeuchi, T. Akiho, K. Sueoka, R. H. Hauge, F. Léonard, and J. Kono, Sci. Rep. **3**, 1335 (2013).
[26] X. He, N. Fujimura, J. M. Lloyd, K. J. Erickson, A. A. Talin, Q. Zhang, W. Gao, Q. Jiang, Y. Kawano, R. H. Hauge, F. Léonard, and J. Kono, Nano Lett. **14**, 3953 (2014).
[27] X. He, F. Léonard, and J. Kono, Adv. Opt. Mater. **3**, 989 (2015).
[28] X. He, W. Gao, L. Xie, B. Li, Q. Zhang, S. Lei, J. M. Robinson, E. H. Hároz, S. K. Doorn, W. Wang, R. Vajtai, P. M. Ajayan, W. W. Adams, R. H. Hauge, and J. Kono, Nat. Nanotech. **11**, 633 (2016).
[29] L. M. Ericson, H. Fan, H. Peng, V. A. Davis, W. Zhou, J. Sulpizio, Y. Wang, R. Booker, J. Vavro, C. Guthy, A. N. G. Parra-Vasquez, M. J. Kim, S. Ramesh, R. K. Saini, C. Kittrell, G. Lavin, H. Schmidt, W. W. Adams, W. E. Billups, M. Pasquali, W.-F. Hwang, R. H. Hauge, J. E. Fischer, and R. E. Smalley, Science **305**, 1447 (2004).
[30] V. A. Davis, L. M. Ericson, A. N. G. Parra-Vasquez, H. Fan, Y. Wang, V. Prieto, J. A. Longoria, S. Ramesh, R. K. Saini, C. Kittrell, W. E. Billups, W. W. Adams, R. H. Hauge, R. E. Smalley, and M. Pasquali, Macromolecules **37**, 154 (2004).
[31] V. A. Davis, A. N. G. Parra-Vasquez, M. J. Green, P. K. Rai, N. Behabtu, V. Prieto, R. D. Booker, J. Schmidt, E. Kesselman, W. Zhou, H. Fan, W. W. Adams, R. H. Hauge, J. E. Fischer,

Y. Cohen, Y. Talmon, R. E. Smalley, and M. Pasquali, Nat. Nanotechnol. **4**, 830 (2009).

[32] B. C. St-Antoine, D. Menard, and R. Martel, Nano Lett. **11**, 609 (2011).

[33] See Supplemental Material at http://link.aps.org/supplemental/10.1103/PhysRevMaterials.2.015201 for a detailed description of the operation mechanism, ultrabroadband response, noise performance, energy harvesting capability and washability of the CNT-fiber detector.

[34] K. Erickson, X. He, A. A. Talin, B. Mills, R. H. Hauge, Y. Kawano, J. Kono, and F. Léonard, ACS Nano **9**, 11618 (2015).

[35] D. Tristant, A. Zubair, P. Puech, F. Neumayer, S. Moyano, R. J. Headrick, D. E. Tsentalovich, C. C. Young, I. C. Gerber, M. Pasquali,, J. Kono, and J. Leotin, Nanoscale **8**, 19668 (2016).

[36] A. Zubair, D. E. Tsentalovich, C. C. Young, M. S. Heimbeck, H. O. Everitt, M. Pasquali, and J. Kono, Appl. Phys. Lett. **108**, 141107 (2016).